



# A review on surface deformation evaluation using multitemporal SAR interferometry techniques

Monika Besoya<sup>1</sup> · Himanshu Govil<sup>1</sup> · Pralay Bhaumik<sup>1</sup>

Received: 9 January 2020 / Revised: 20 June 2020 / Accepted: 10 July 2020 / Published online: 14 August 2020  
© Korean Spatial Information Society 2020

**Abstract** Deformation monitoring is a crucial matter to avoid catastrophic failure due to extraction of resources. Radar data, mainly synthetic aperture radar (SAR) data and their diverse techniques are suitable for deformation monitoring. This paper provides a review of SAR data and their techniques for deformation monitoring. It also provides a brief description of Image acquisition, SAR geometry, SAR development, satellite specifications, and commercial software used for Interferometry and deformation monitoring. In the end, it is concluded that the existing SAR techniques are capable of accurate monitoring of land deformation. It is also concluded that persistent InSAR (PSInSAR) gives better results than differential InSAR (DInSAR).

**Keywords** Deformation monitoring · SAR · InSAR · DInSAR · PSInSAR

## 1 Introduction

Deformation is the alteration in shape or dimensions of an object as a result of the application of stress to it. Distortion, rotation, movement and shape change that occur in a system are known as deformation [1]. It introduces due compression, extensional and shear stress as demonstrated in Fig. 1. Compression stress leads to the formation of compacting rocks, extensional stress breaks rocks, by pulling force and shear stress forces rocks to sling

horizontally past another [1]. Deformation can be vertical (90°) and horizontal (nearly 1°) along the dip line [1]. It can occur immediately or can be delayed for a long period, and it can occur over a small or a large area. Subsidence may occur at low rates ranging from a fraction of an inch to as much as 3 inches per year [2].

Land deformation may be caused by extraction [3] of resources from the ground such as water, minerals, natural gases, oil, construction defect, soil contraction, earthquake, soil erosion, landslides, contraction of the root of tree and shrub, etc [3]. It forms buoyancy, which fails to support overburden or external pressure. If it is in the form of subsidence, then it becomes a serious economic, engineering and environmental issue [4].

Mines are of two types- one is opencast and another is underground. Mining inflicted deformation, which is a major problem in the form of subsidence, is noticed worldwide. It is a result of readjustment of collapsed mine voids, because of overburden on the surface after extraction of underground mineral [5] from the mines. If the movement is lateral or vertical in the mine, then it is called mine subsidence. Subsidence in mine is gentle and gradual settling of the earth plane [6] or deformation or movement (vertical or downward) of the earth. However, mine subsidence cannot be induced by the earthquake, soil erosion, volcanic explosion, contraction of roots of trees and shrubs, soil settling, landslide, soil thawing and freezing, rapid transit tunnels, faultily compacted soil, or collapse of the storm and sewer drains [7]. Subsidence in coal mines can be of three types, viz. (a) crack, fissures or step fracture (b) pits or sinkhole or pothole and (c) sag or trough subsidence [6] as shown in Fig. 2. Subsidence occurs mainly in underground mines [7]. Cracks are primary indicators of deformation in an area. Deformation can be slow or rapid, but it is a gradual process in the context of the extracted

✉ Monika Besoya  
geniousmonika11@gmail.com

<sup>1</sup> Department of Applied Geology, National Institute of Technology, Raipur 492010, Chhattisgarh, India

**Fig. 1** Each rectangle presents the system or rock, which is under deformation due to stress (left) represent stress types, and (right) distortions occur in rocks

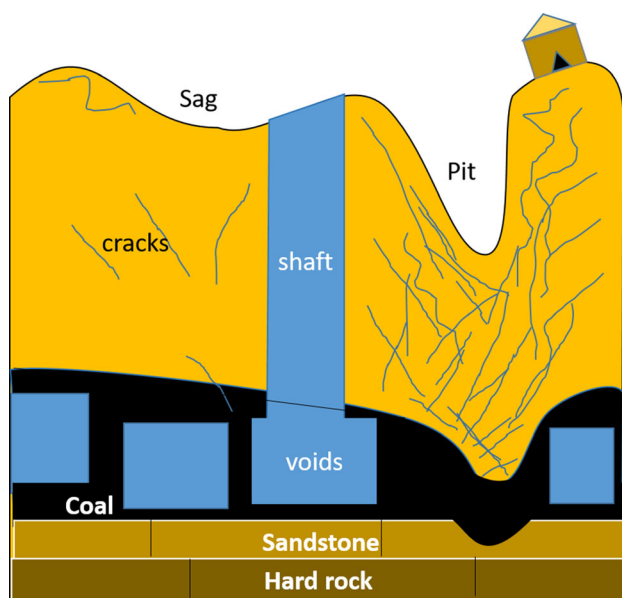
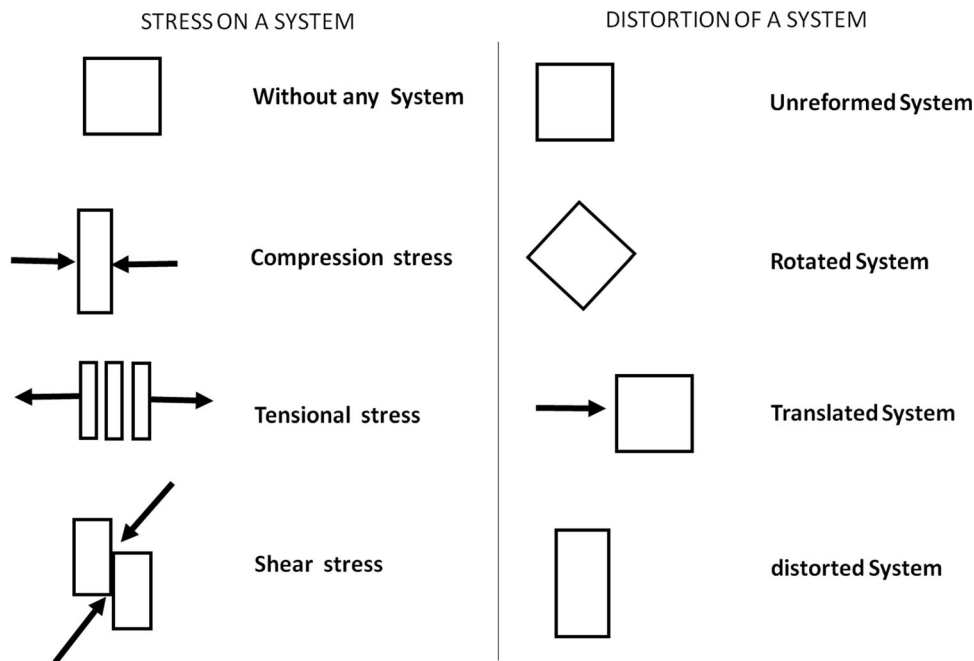


**Fig. 2** An illustration represents type of subsidence in coal mine

resource. The deformation affected surface areas are generally larger than the resources extracted areas. Undue aspirations to extract minerals beyond some threshold depth have posed the problem of mine subsidence. Hence, from the safety point of view, there is a significant demand to monitor the mines routinely. Many complications occur in mines due to mining activities, for example, gas and water-related problems, mine surface deformation, subsidence, instability of mine overburden (OB) dump [8], risk of health and safety of miner, environmental issues, reform

issues of mine land etc. The deformation not only impacts living beings but also the surrounding environment [9] due to the release of toxic gases [10], soil change, land degradation, etc. Subsidence cannot be eliminated, however, it can be reduced significantly and the affected areas can be condemned for residential use or for other engineering constructions. The subsidence or deformation surveys are expensive when they are carried out through the traditional methods. These traditional surveys are performed on the as-less-as-possible basis [6], only on selective sites [6] of important engineering construction [11], and usually twice annually in the selected sites.

The subsidence measurements depend on the detection, assessment, and evaluation of the past and future deformation [12]. The traditional techniques used for mining subsidence are GPS survey, levelling survey [13] and aerial photographs [14] on localized areas. These techniques are tedious and time-consuming, with small area coverage [15]. Due to these limitations, the old methods are being phased out and being replaced by the latest remote sensing techniques. Today's advanced remote sensing techniques can measure minute subsidence with millimetre to centimetre-level accuracy [16, 17], while for point bases the level of accuracy varies within 0.1–5 mm [18].

Remote sensing is effectively implemented for solving challenges in most scientific disciplines like climate change, disaster monitoring, megacities monitoring, resource management, subsidence monitoring, disaster monitoring, traffic monitoring, target detection, etc. [19, 20]. In this remotely sensed world, two different types of instruments, namely imaging sensors and non-imaging

sensors, are continuously monitoring the earth. In this direction, RADAR is an invention that has changed the human race by providing a fine-resolution image from electromagnetic radiation [21]. In the case of imaging sensors operating in the optical wavelength, cloud cover is a major hindrance, but imaging radars are equally capable under cloudy conditions because of their cloud-penetrating wavelength. In the polar regions and regions with perennial cloud cover, for example in the region between 15° latitudes [21], radar plays a tremendous role. It cuts all barriers of atmosphere and illumination source (day-night data acquisition capability). Imaging radar has two major functions—(a) mapping the topographic feature present in the target area and (b) measuring geodetic location in three dimensions from the platform [21].

The World's first synthetic aperture radar (SAR) satellite for civilian applications with a resolution of 20–30 m and swath 100 km was launched on 26 June 1978 [22] for mapping and monitoring of agriculture, deforestation, sea ice, ocean wave [23] etc. Today there are many satellites through which it is possible to acquire radar data for various applications of earth observation and monitoring. Some of the space missions have already completed their life span, for example, SEASAT, ERS-1 (1991–2000), ERS-2 (1995–2011), ENVISAT (2002–2012), ALOS-1, etc.

SAR mission and techniques played a major role to detect and monitor deformation. The basic techniques that are being used for prediction and monitoring of the earth are interferometry (InSAR) [11], differential interferometry (D-InSAR) [24], persistent scattering interferometry (PSInSAR) [5] and ground-based InSAR (GBInSAR) [25, 26]. The two-wave radar interferometry technique utilizes the coherence properties of electromagnetic radiation. SAR interferometry is useful for regional-scale monitoring and mapping. The short temporal interferogram is used for vegetation change detection, while long-term interferogram is used to detect surface deformation [27]. Today we have several options of radar satellites, which are capable of coherent image acquisition. One can use data from these satellites to carry out SAR interferometry for deformation monitoring. Data from some of these satellites are easily accessible, for example, (a) European Remote Sensing satellites (ERS1/2)—launched on 1991/1995 [6], (b) Environmental Satellite (Envisat)—Advance Synthetic Aperture Radar (ASAR) SAR sensor operated in C-band, operational from 1 March 2002 to 8 April 2012, (c) TerraSAR-X (TSX)—operating in X band [28], (d) Japanese Earth Resources Satellite 1 (JERS-1)—Japan's Advanced Land Observation Satellite (ALOS) whose SAR sensor is phased array type L-band synthetic aperture radar (PALSAR) [29, 30] (e) RADARSAT-2

[31, 32], and (f) Sentinel 1/2—operating in C band [33, 34, 35, 36] etc.

## 2 Synthetic aperture radar (SAR) basics

To know the process of deformation monitoring, it is a necessity to know what SAR is and how it works for monitoring of deformation. During its initial days, microwave remote sensing was used in the form of a non-imaging radar system for detecting an object. During the Second World War, radars were extensively used to track enemy planes and remote sensing was used as much for imaging [37]. Since 1950, SAR (synthetic aperture radar) has become a major part of radar remote sensing [23] due to its ability to capture high-resolution imageries over a wide swath without much conflict with the atmospheric conditions. Radar has played an important role in monitoring the changes on earth by acquiring imageries since the 1970s. Radar remote sensing plays an important role in the planetary study [38], for lunar topography [39], topography mapping of the earth [21] and many other applications.

Radar is a tool based on the principle of echolocation [40], by measuring the backscattered echoes or signals from the target to the sensor. SAR is an active imaging sensor and a powerful instrument for monitoring the earth remotely. It can be mounted on ground or aircraft or satellite, and thus operate as a means of ground-based or airborne or space-based remote sensing respectively. SAR sensors operate in the microwave region of the electromagnetic spectrum, about 1 mm to 1 m in wavelength, as shown in Table 1, though ranges of individual bands vary from literature to literature. SAR captures the amplitude and phase information of the electromagnetic radiation. SAR sensor images provide information about the earth's surface, which is different from information acquired through other regions (visible, thermal, etc.) of the electromagnetic spectrum. With the help of Doppler's effect principle, the real aperture radar (RAR) can be used to synthesize a long antenna to form a high-resolution synthetic aperture radar. High resolution airborne SAR data are used for the purposes of military surveillance and geophysical monitoring.

### 2.1 Image acquisition

The SAR antenna transmits microwave frequencies with the help of the transmitter and captures the stream of echoes coherently and separates these echoes into individual echo with the help of the receiver [41]. In a standard SAR sensor, the SAR antenna can image the earth by three modes of acquisition (a) strip map, (b) scanSAR, and

**Table 1** Commonly used wavelengths in a SAR sensor with respective frequency description

Frequency band	Ka	Ku	X	C	S	L	P
wavelength ( $\lambda$ ) (cm)	7.5–1.2	1.7–2.5	2.5–4	4–8	8–15	15–30	30–100
Frequency ( $\nu$ ) (GHz)	40–25	17.6–12	12–7.5	7.5–3.75	3.75–2	2–1	0.5–0.25

(c) spot-light (high resolution) mode [41]. SAR antenna acquires an image in the form of backscattered signals. SAR backscattered image has the backscattered energy of the terrain (scatterers) in the form of a complex number, which carries information of phase and amplitude values corresponding to each respective pixel of an image, i.e. corresponding to each resolution cell on the ground [42]. Amplitude depends more on the backscattering property of the scatterer on the ground, and not the chemical composition of the scatterer [42]. Radar waves propagate with the speed of light ( $3 \times 10^8$  m/s) to impinge any target and come back with the same speed. This speed provides the measurement of distance ( $\Delta\text{time} \times \text{velocity}$ ) in terms of half of the travel time. Radar measures any distance using the delay of time between transmitting and receiving of the radar pulse.

There are more backscattered informations from a rough surface rather than a smooth surface, because the radiation is mirrored away from smooth surface due to specular reflection. High backscatter (from the urban area, exposed rock, etc.) is represented by a bright pixel in an image, while low backscatter is represented by dark colour pixel in an image. In any coherent image, the presence of several scattered returns generated from each resolution cell appears like salt and pepper. This phenomenon, commonly present in all SAR images, is called the speckle effect. The speckle effect degrades the excellence and effectiveness of SAR images and hence needs to be eliminated. It is achieved by using multiple images or images from different look angle, which are then averaged out to cancel the inconsistencies, keeping the unvarying amplitude level untouched [42].

Two independent observables, measured by SAR sensor, are amplitude and phase of the backscattered echo. Most SAR sensors are capable to acquire these data over a wide swath of 10–400 km and pixel resolution of 1–100 m, depending upon the mode of acquisition. The amplitude of an image pixel is the terrain backscattered energy of corresponding ground cell, which has been sent back to the antenna [43] to form the image. Amplitude information is used for the study of the land cover classification, soil moisture content, oil spill detection, etc. Phase data measure the wavefront that is a fraction of the backscattered radar wavelength, at the time of capture by the antenna. Phase information is used to monitor or detect changes in the order of centimetre over the vast land surface [44]. The interaction of radar signals with the ground surface is a complex process because it depends on (a) physical

properties of the constituent material such as dielectric constant (depends on moisture content), (b) geometric factors (slope, orientation, surface roughness, etc.), (c) wavelength [45] and (d) slant range at which the absorption and scattering are taking place [43].

## 2.2 SAR geometry

SAR data have two types of resolution of a pixel. The first one is along the direction of flight, which is known as azimuth resolution and the second one is across the direction of flight, which is known as range resolution. Measurement of the slant range and azimuth range in a resolution cell depends on features of the SAR system [42]. The angle between the range direction and the nadir is the look angle, and the angle between the range direction and the local perpendicular to the resolution cell is called the incidence angle [35]. Each pixel has a different incidence angle because of the range direction and local surface undulation. The incidence angle for a perfectly smooth surface is equal to the look angle. The angle between the range direction and the horizontal line is called the depression angle.

Due to angles and undulation (slope) in terrain, SAR images have distortions known as layover (tall objects and steep slopes appear laid on ground), foreshortening (slopes facing toward the radar appear compressed and length measurements are incorrect) and radar shadow (areas occulted by other areas, which increase with the increment in the incidence angle) [42, 35, 46]. Radar images, and in turn interferograms generated from them, are distorted by slant range distortions. So for interpretation of interferograms, we must know the geometry of the general area of study. These distortions can be corrected by ascending (upward scanning, i.e. south to north) and descending (downward scanning, i.e. north to south) image acquisition by the SAR antenna (pointing towards the same side (say, right) of the direction of movement) [42].

## 2.3 Development of SAR sensors

SAR sensors primarily operate in P, S, L, C, and X bands [36]. X band data is mainly useful for forest volume mapping [47] because leaves reflect shorter wavelengths, C band data are used for land deformation [48], L band data are used to study geology beneath the canopy and P band data are mainly useful for flood water mapping [49]. SAR satellites are operated by different agencies. For example,

(a) European Space Agency operates the ERS-1 and 2, Envisat and Sentinel-1 and 2, (b) Japan Aerospace Exploration Agency (JAXA) operates JERS-1, ALOS-1 and ALOS-2, (c) Canadian Space Agency (CSA) operates Radarsat-1, Radarsat-2 and the upcoming Radarsat constellation, (d) Deutsches Zentrum für Luft- und Raumfahrt (DLR) operates TerraSAR-X and TanDEM-X, (e) Indian Space Research Organization (ISRO) operates RISAT-1 (fully polarised), NovaSAR-1, upcoming NISAR (with NASA), (f) Comisión Nacional de Actividades Espaciales operates SAOCOM, (g) Italian Space Agency (ASI) operates COSMO-SkyMed, (h) Instituto Nacional de Técnica Aeroespacial (INTA) operates PAZKorea, (i) Aerospace Research Institute (KARI) operates KOMP-Sat-5. Apart from these, the National Aeronautics and Space Administration (NASA) of USA operates several satellite-based SAR sensors. NASA is also part of project NISAR with Indian Space Research Organisation (ISRO), for development of SAR sensors operating in L and S bands.

### 3 SAR techniques used in deformation monitoring

SAR, in general, is based on the Doppler Effect theory. The principal of SAR is to synthesize large aperture by storing the successive echoes from moving radar to achieve the high spatial resolution [23] in azimuth (along-track direction) and slant-range (cross-track direction) directions [50]. The slant range resolution ( $\Delta R_R$ ) is  $c\tau/2$ , where ' $\tau$ ' is the pulse width and  $c$  is the speed of light [51]. Azimuth resolution is  $\lambda R/L$  where  $\lambda$  is wavelength of the radar pulse [46]. SAR data are broadly used for two techniques—polarimetry and interferometry. Polarimetry deals with the full vector nature of the data or polarization of the backscattered echo to retrieve a geophysical property of scatterers. On the other hand, interferometry deals with the phase information (slightly different position) to retrieve the topographic three-dimensional feature [52]. SAR interferometry is a well established powerful tool in remote sensing [53], which has been extensively applied to measure accurate geophysical parameters in the last 35 years [54]. It gives high accuracy to measure the third-dimensional (height or elevation) measurement for minute transformation [55]. This paper mainly focuses on the basics of InSAR and deformation monitoring techniques. The contemporary techniques of interferometry used to monitor deformation are DInSAR and PSInSAR. Interferometry was first introduced for mapping of the planetary surface. Venus surface was mapped by Arecibo interferometer at 70 cm wavelength by Campbell and his co-workers in 1970 [56], and then lunar topography was mapped in 1972 by Irwin I. Shapiro and his co-workers by

using radar photography [39]. In 1974 Graham used RAR antenna at slightly different positions to monitor the three-dimensional topography using interferometry in slant range direction [21, 44]. InSAR is a monitoring tool, introduced in the late 1980s [57], which predicts remotely by sensing small changes in the earth's height at a record level of spatial detail [58]. A detailed review of radar interferometry has been explained nicely in [59–61].

#### 3.1 Interferometric SAR (InSAR)

Interferometry is a technique that utilizes the principle of interference of wave. By using two light waves from a coherent source two images are acquired, which are superimposed to cause interference to take out information. The principle of interferometry is accomplished by using a coherent source of data. The interferogram is dependent on the radar parameters and target properties. SAR interferometry can be achieved along-track and across-track [62]. Interferometry has been used for deformation and planetary motion since 35 years. It is used to extract deformation of earth due to volcanic eruption [63], landsliding [64], surface subsidence [65], urbanization [66], mining [48], oil extraction [67] etc. Mapping of surface geology [68] has been done by using interferometry.

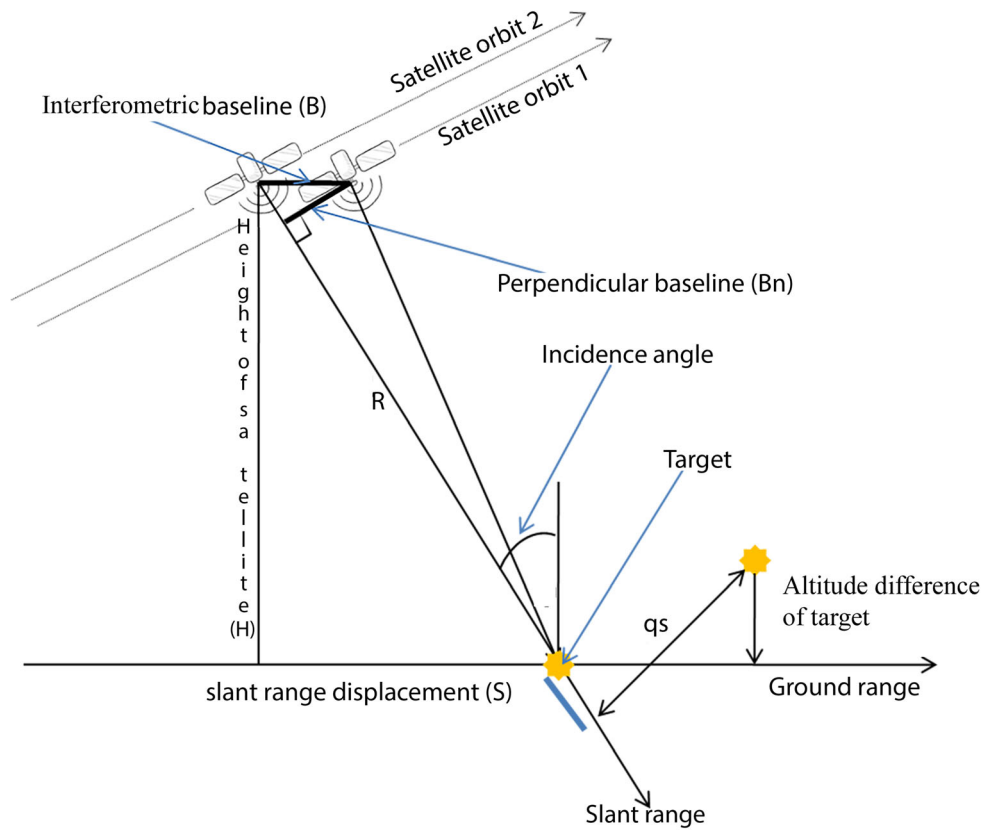
##### 3.1.1 Basic process of interferogram formation

The deformation of an area is measured by acquiring two coherent images, and then by detecting targets present in a particular resolution cell in each image. The SAR source observes a target area from slightly different look angles as shown in Fig. 3. Using two SAR images (master and slave images), suppose amplitude of target (point scatterer), which is present in the first image resolution cell, is the same as that in the respective resolution cell of the second image. By observing the common target in the images, having the same amplitude in both the images (not changed over a period), the change between others can be easily identified with the help of the common target within the resolution cell. Interferograms are generated by the first image pixel and the complex conjugate of the corresponding pixel of another image, which means the images are processed pixel by pixel [43, 44].

The coherence or interferometric correlation is the main criterion for interferometry [62]. Two coherent SAR images of the target or area (common in both images), used to form interferogram, can be acquired during a single-pass called simultaneous interferometry (both acquisitions at the same pass with slightly different positions) or by the repeat pass (different acquisition by the same SAR sensor at different passes). Then these images are co-registered and the phase difference ( $\varphi$ ) pattern of the corresponding pixel



**Fig. 3** Geometric parameters of the satellite interferometry SAR system for deformation monitoring (modified from [69])



elements (which is a function of interferometric baseline, orientation, wavelength and target height) is estimated at the base for the fringe formation [23]. The interferometric baseline can be calculated by two methods - single pass or one-pass method (both the transmitting and receiving antenna set on the same base) and two passes method (the transmitting and receiving antenna set on altered bases) [62].

The path difference is the variation in the length of coupled waves, which have traveled from source to impinge the coherent target, whereas phase difference is the shift in wavefront from the origin. It is helpful when there are two waves, in which one starts from zero and another wave having some non-zero position at the same time. Suppose, two different waves (S1 and S2), are meeting at a single point (P), then the path difference will be equal to  $S_2P - S_1P$  Fig. 4.

If a wave travels an extra length, then there will be a difference in phase  $\varphi = 2\pi \times \text{path difference}/\text{wavelength}$ . The phase change of wave is proportional to the distance traveled (during transmission and reception). It can be calculated [23] as

$$\varphi = 2\pi r/\lambda \tag{1}$$

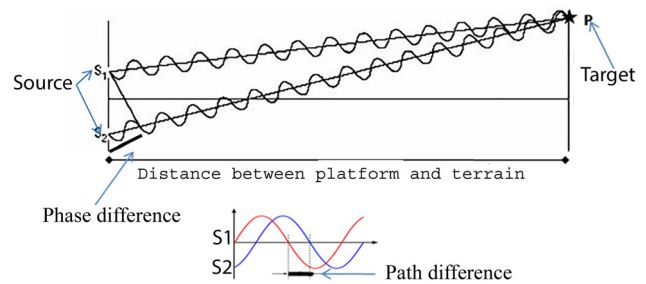


**Fig. 4** Illustration of the path difference of coherent waves

If the phase change is zero and total distance traveled is  $R$  (transmitting) +  $R$  (receiving) =  $2R$ , then the phase is equal to

$$\varphi = 2\pi \times 2R/\lambda = 4\pi R/\lambda \tag{2}$$

where  $\varphi$  is the phase change between the two way traveling and,  $R$  is the transmission or reception distance.

The path difference ( $\Delta r$ ) can be calculate by using geometric parameters such as perpendicular baseline ( $B_n$ ), slant range distance between target and sensor ( $R$ ) and the perpendicular displacement of the resolution cells along the slant range ( $q_s$ ). The interferometry phase varies with path difference/wavelength ( $\lambda$ ) [42].

$$\Delta r = -2B_n q_s/R \tag{3}$$

Then phase difference is equal to

$$\Delta\varphi = 2\pi\Delta r/\lambda = 4\pi B_n q_s/\lambda R \quad (4)$$

Any factor (land displacement, moisture content, etc.) or condition (snowfall, land change, etc.), which disturbs the backscattered signals, will also affect the fringe of the interferogram. This can be calculated and measured by InSAR technique [43]. The perpendicular baseline is determined from orbital information.

The relative terrain proportional phase map generated by interferogram flattening is computed by

$$\Delta\varphi = (4\pi B_n q/\lambda R) - (4\pi B_n S/\lambda R \tan \theta) \quad (5)$$

where  $q$  is the altitude difference between point targets from the horizontal plane.

Subsequent steps in a typical analysis are- Phase filtering (for better visualization of results) and Phase unwrapping (for accurate and unambiguous measurements from the interferogram). Advanced InSAR techniques provide better results for the evaluation of deformation over an area.

### 3.2 DInSAR technique for deformation monitoring

In the case of DInSAR, an area is imaged at two different points of time to monitor even the slightest of change on the ground surface due to any cause. The interferogram represents the phase difference of pixels of one image from the corresponding pixels of another image [43, 44]. The two SLC or raw images (master and slave images) of a desirable area (area of interest) are used to estimate the baseline. The co-registered images are then used to generate an interferogram by calculating phase difference pixel by pixel followed by flat earth correction, phase unwrapping and then geocoding [70]. The interferogram obtained after flat earth correction is wrapped (contains phase difference values  $0 - 2\pi$  only), hence it needs to be unwrapped (to reveal true phase difference values beyond  $2\pi$ ). Phase unwrapping is an essential procedure for deformation analysis [62], where one has to derive height displacement in the cross direction (slant range) of the antenna [18]. The displacement phase unwrapping is derived from  $4\pi/\text{wavelength} (\lambda) \times \text{height displacement}$  [18].

The phase components information contributes to the interferogram generation. The phase measurement depends on how good the images are co-registered. The phase change in the interferogram is the composite of topographic information ( $\varphi_{\text{topo}}$ ), surface dislocation between the two acquisitions ( $\varphi_{\text{disp}}$ ), atmospheric delay ( $\varphi_{\text{atmo}}$ ), and noise ( $\varphi_{\text{noise}}$ ) [18], as shown below in the equation.

$$\varphi = \varphi_{\text{topo}} + \varphi_{\text{disp}} + \varphi_{\text{atmo}} + \varphi_{\text{noise}} \quad (6)$$

The formation of the interferogram depends on the line of sight (LOS), the slope of the area, the angle of incidence, the topographic difference from two slightly different positions of radar, sensor configuration, etc. In an interferogram one fringe is equal to one half of the wavelength. Narrow fringes clearly show the undulations in terrain [50]. Interferogram can be used to interpret many types of deformations that occur in the area. If the surface changes due to the growth of vegetation, snowfall, flood, geological hazard, etc., then the interferogram also changes due to phase disturbance.

Accuracy of interferometric analysis gets degraded due to loss of coherence by temporal and geometric decorrelation, atmospheric artefacts, residual orbital components and uncompensated topography affecting the phase of two acquisitions. To remove these limitations advanced interferometric techniques are introduced. These techniques work on stacks of images, and some designated permanent points (PS points) in these images, to estimate the deformation.

### 3.3 Persistent scatter interferometry (PSInSAR)

The PSInSAR technique was developed at the Politecnico di Milano (Milan, Italy) [12]. In the last 20 years, it has been used to detect and monitor small or minute surface deformation. PSInSAR is a competent technique of remote sensing [2, 73, 74], which utilizes the natural and anthropogenic target properties to detect a coherent change over a long time [16]. This is achieved through analysis of amplitude-time series, after radiometric correction [75].

The PSInSAR method uses the temporal and spatial characteristics of designated targets or so-called persistent scatterers (PS) [75] and provides a precise estimation of total phase difference in terms of deformation, atmospheric, topographic and orbital phase [10]. PSInSAR has three requirements in the area of interest- the maximum number of images, slow target motion and a sufficient number of PS points [75]. The designated PS points can be building, bridge, coal mine site etc., which have not changed in a while. To increase PS points artificial corner reflectors can be used because they give high backscatter [49].

#### 3.3.1 Phase scatterer detection

Many attempts have been made to improve the selection criterion for PS points. The PSInSAR method incorporates three such criteria, namely, phase stability, correlation and normalized amplitude dispersion [74].

Amplitude dispersion  $D_A$  can be written as [74].

$$D_A = \sigma_A/m_A \quad (7)$$

where,  $\sigma_A$  and  $m_A$  are standard deviation and mean of the backscattering intensity. In this method, Ferretti [74] pointed out that a pixel with a D-value between 0.25 and 0.4 can be selected as PS point. In this criterion phase information is not required. Hence it is easy to implement, it has excellent efficiency and there is no relationship among adjacent pixels. So it is useful to detect the singleton PS point.

Amplitude stability index (ASI) for detection of PS point is defined by using Eq. (8) [76].

$$ASI = 1 - (\sigma_A/m_A) \quad (8)$$

PS points are selected based on some threshold value. Atmospheric phase screen (APS) introduces phase ambiguity due to delay caused by atmospheric disturbance. This is estimated and then removed from the generated image. DEM is used to remove the topographic phase signature from interferogram. For high coherence, PS points create a network with the neighboring PS points. These PS points are then used to calculate deformation in the LOS.

The main limitation of PSInSAR is that it measures cumulative ground movement in the LOS, and does not measure the non-linear movements which occur due to geological processes [65].

PSInSAR is an advanced interferometry technique, which has been used for the deformation monitoring in areas in the USA using ERS1/2 [77] and in China [10]. In literature, the PSInSAR technique has been used for some novel findings. Subsidence, at a rate of 44 mm/year, was detected in the Zonguldak province of Turkey using 18 ascending SAR images (January 2007 to June 2010) of ALOS data [68], the Karadon and Uzulmez mine galleries were located by PSInSAR technique [78], and coal mining areas of India were found to experience subsidence, at a rate of 20 mm/year, using 17 C-band Sentinel-1 images [48].

#### 4 Software for interferometry

Radar remote sensing provides a new platform for earth science research that increases the productivity and lowers the risk. However, suitable digital data sets and appropriate software remain the pre-requisites for any remote sensing project. InSAR analysis can be performed on freely available SAR data sets and open source or commercial software. The freely available software packages are mostly used for academics.

Much open source software is available now, as described in Table 2 below.

Repeat orbit interferometry PACKage (ROI\_PAC) is a powerful open-source software developed and maintained by Jet Propulsion Laboratory (JPL/Cal tech) [79], Delft Object-Oriented Radar Interferometric Software (DORIS) is developed by the Delft Institute of Earth Observation and Space Systems of Delft University of Technology which can handle data from ERS, ENVISAT, JERS, etc.

DInSAR technique can be performed by the SUBSOFT software, developed by the remote sensing laboratory (RSLab) group from the Universitat Politècnica de Catalunya (UPC). This software is based on the use of Coherent Pixels Technique (CPT) algorithm [80].

Generic mapping tools synthetic aperture radar (GMTSAR), is written in C programming language ANSI C standard, which can perform pre and post-processing operations on ERS-1/2, JERS-1, SIR-C/X-SAR, RADARSAT, ENVISAT ASAR, ALOS-1, TerraSAR-X, COSMOS-SkyMed, Radarsat-2, Sentinel-1A/B, and ALOS-2 data. The results are shown or displayed as postscript files and KML images for Google Earth [81].

The three Sentinel toolboxes Sentinel-1, 2 and 3 are on the common platform SNAP, which is a community developed by ESA to access the software and share the knowledge for promoting the results and achievements. The ESA toolboxes provide support for the ERS-ENVISAT missions, the Sentinel 1/2/3 missions and a range of other missions for the scientific exploitation [82].

Gamma SAR interferometry software is a user-friendly, full functionality, command-based software having compatibility with UNIX operating system, PC/LINUX, and PC/NT [83, 84]. It is a bundle of packages like Modular SAR Processor (MSP), interferometric SAR processor (ISP), differential interferometry and Geocoding Software (DIFF and GEO), Land Application Tools (LAT), Geocoding and Image Registration software (GEO), and interferometric point target analysis (IPTA). It supports the entire process flow from raw data to final product to be generated from any of the sensors like ERS-1/2, ENVISAT ASAR, Radarsat-1/2, Sentinel-1A/1B, JERS, ALOS PALSAR-1/2, SIR-C, TerraSAR-X, Tandem-X, Cosmo-Sky-med, KOMPSAT 5, RISAT and NASA-JPL UAVSAR [85].

PolSARpro is developed by the IETR (Institute of Electronics and Telecommunications of Rennes—UMR CNRS 6164) of the University of Rennes, France. IETR is in charge of the development of the PolSARpro software, under ESA since 2003. It aims to facilitate research by providing the processing capability of all type of data from Sentinel-1, ALOS-1 PALSAR, ALOS-2 PALSAR, COSMO-SkyMed, RADARSAT-2, RISAT, TerraSAR-X and Tandem-X [86].



**Table 2** Description of open source and commercial software

Software	Developer/company	Package
Gamma	Gamma remote sensing	Commercial
ENVI SARscape	Exelis	Commercial
DIAPASON	Altamira	Commercial
IMAGINE radar mapping suite	Erdas	Commercial
ISCE	Caltech/JPL and Stanford (UNAVCO manages licensing and distribution on behalf of WInSAR)	Open source
ROI_PAC	Caltech/JPL	Open source
GMTSAR	SIO and SDSU	Open source
DORIS	TU-Delft	Open source
Sentinel-1 toolbox	European Space Agency	Open source
OSARIS	Loibl and his coworkers	Open source
LiCSBAS	Morishita and his coworkers	Open source

LiCSBAS is an open-source SAR interferometry time series analysis package that integrates with the automated Sentinel-1 InSAR processor LiCSAR. It utilizes liberally available LiCSAR products, and thereby saves user processing time and disk space while obtaining the results of InSAR time series analysis [87].

Two more commercial software, namely the SARscape and Sarproz, are used for interferometry these days. SARscape is a commercial software, which was developed by Sarmap (a Swiss company). It interfaces with the ENVI image analysis software. ENVI SARscape software processes all types of airborne and spaceborne SAR data.

The Sarproz software was developed by Dr. Perissin [88]. It is a powerful, multifaceted software, based on the Matlab. It is user-friendly (no requirement of coding knowledge), can run on multiple CPU cores or computer clusters automatically, and can support data from most of the radar satellites like TerraSAR-X [28], ALOS [89], etc. It can process all interferometric modules (InSAR, DInSAR, PSInSAR, etc.) [90] and can be used for monitoring subsidence [88]. For more details about SAR software, utility, materials, and libraries refer links available on geospatial warehouse [91].

## 5 InSAR advantages and limitations

The InSAR technique is fast and economically good as compared to traditional techniques. It is a software-based method, which consumes less manpower. High precision (less than centimeter) in deformation monitoring and high accuracy in target georeferencing can be achieved using PSInSAR technique [29]. The results provide information,

which is continuous and reuseable for further study over the same area.

One of the limitations of InSAR techniques for accurate deformation measurement lies in the availability of data with suitable coherence, atmospheric stability and orbit information. These are required for the procedure to return a good interferogram as shown in Eq. (6). The loss of coherence occurs due to geometric and temporal decorrelation of two acquisitions. As a result, the reflectivity also changes, which affects the phase difference for generation of interferogram [12]. Data sets having good coherence are trustworthy for interferogram. Coherence maps are also used as an indicator for LOS deformation monitoring. To overcome the problem of decorrelation, short temporal baseline and short perpendicular baseline images should be taken to minimize temporal and geometric decorrelation respectively [12]. Besides, care should be taken to minimize atmospheric artifacts, which occur due to presence of different meteorological conditions [12]. Orbital information plays a vital role in the estimation of flat earth phase. So all the processing steps depend on the geometry and acquisition period of images.

Another limitation of InSAR techniques is data archive, as more data sets are required for better accuracy. Availability of suitable interferometric data can not be assured only by temporal resolution over some time. ALOS Palsar L band data are available with 35 days repeativity. Sentinel-1 A data are available with 12 days repeativity, and in conjunction with the Sentinel-1 B data temporal resolution reduces to 6 days. The data sets are used as per the topography of the area of interest, for example, L band data can penetrate vegetation canopy, but C band data cannot. So it is not always possible to get archival data over an area with the required baseline measurement and

wavelength. To reduce these drawbacks, different approaches have been proposed to detect the deformation over an area.

## 6 InSAR application in deformation monitoring

In this section, a concise review of InSAR techniques is furnished for application in deformation monitoring. Deformation is the change of the earth's surface. It can occur due to loss of elevation, gradual change due to shrinkage or movement of earth's surface material caused by the motion of the surface or loss of the subsurface support. The deformation of the earth's surface is a universal problem in the form of subsidence. Primarily radar interferometry was used to monitor the deformation in the 1980s [92] for the detection of small changes.

According to the geological survey of the US in 1991, sustainable development of land and water depends on improved scientific understanding and detection of subsidence of our land and water resources [3]. Scientific literature conveys that InSAR is important for many applications like the production of the DEM [93]. With advancement or extension of InSAR, DInSAR and PSInSAR have been used to [94] monitor the surface deformation caused by natural [64] and anthropogenic activity. InSAR techniques are widely used to measure the topographic profile, surface deformations, or dielectric properties of the ground surface [2, 4, 23, 72], and subsidence monitoring [16, 88]. InSAR is capable to measure the elevation change or deformation due to mining activity [11]. It is not possible to measure the full displacement vector along the LOS since radar sensors are only sensitive to vertical surface deformation (away or towards) from the satellite [44, 54]. The 'away' case represents surface subsidence and 'towards' case represents surface upliftment [95]. The measurement of deformation/subsidence is very fast in this method due to the availability of radar data and monitoring techniques. Sentinel-1 C band data, due to its availability, has shown great potential to monitor the deformation of the earth's surface worldwide [29, 48, 96–100].

InSAR technique has been used worldwide for detection of mass movement by using ground-based InSAR (GBInSAR) [101], subsidence detection in wetland [102], subsidence monitoring near intercity railways with multi-temporal InSAR (MTSAR) technique [28], subsidence induced by coal mining [11, 16, 17, 19, 26, 34, 63], etc. The interferogram fringes provide qualitative (shape and extent of subsidence) and quantitative (rate of subsidence between two passes of the satellite) details of the area under study [6]. A detailed review of mine surface deformation monitoring using InSAR techniques is specified in

[103]. Urban deformation due to waterlogging has been monitored by C band Sentinel data using the DInSAR technique [66]. Naturally occurring deformation such as landslide has also been detected in Lower Austria (Austria), Kaohsiung County (Taiwan), South Tyrol and Abruzzo (Italy) and the Lubietova (Slovakia) by using InSAR techniques [64].

In the United States, more than 80% of subsidence occurs due to the shrinking of the earth by extraction and drainage of groundwater or human activities. Surface displacement affects 45 states and more than 17,000 sq. miles [3]. Subsidence is presently dangerous due to the increasing development of land and water [3]. Five areas of California have been studied for subsidence or change in earth surface due to water extraction, the Santa Clara Valley in northern California for subsidence due to agriculture use, Houston–Galveston area in Texas for subsidence due to extraction of oil and gas, and south-central Arizona for subsidence and fissuring of earth surface due to the mining of water [3]. In 1998, with the help of the InSAR technique, subsidence measuring approximately 2 inches was found in Antelope Valley, the Mojave Desert, California for the period October 20, 1993, to December 22, 1995. Subsidence also affects railway tracks, which has been detected by using InSAR techniques [28]. In India, the deformation of land occurs mainly due to the extraction of water [104], mining activities [48], and the development of land [48]. Subsidence has been monitored by C and L band data in the case of coal mines [17, 48] and in case of an urban area [66]. Overall, C and L band SAR data and associated InSAR techniques show great capability in deformation monitoring.

## 7 Conclusions

Earth monitoring through space based visible data has shown its capability in different applications. The visible bands fail to deliver desired results in adverse meteorological conditions like rain, cloud, storms, etc. To overcome these conditions, radar data became a favorable choice for different applications. Radar data are available at different wavelengths. During the initial days radar data were used for monitoring planetary motions. Today, with their present capability and availability, radar data have been converted into an essential tool for monitoring planets and their surface.

With the availability of SAR data, the golden time has started for monitoring of deformation in a more effective and less time-consuming manner as compared to traditional techniques. This paper presents the importance of SAR data and its techniques for an accurate evaluation of deformation.

Using different space-born data and techniques, it is easy to monitor even the smallest of change (less than a centimeter) on earth's surface along the LOS of the radar.

The data is acquired through different agencies as per the availability and application. In SAR images, the penetration becomes deeper while image contrast and noise becomes less with increase in wavelength, and vice versa. C band data is useful for small change detection over less vegetated area and L band data is useful for the highly vegetated area, because L band wavelength can provide earth information underneath the canopy by penetrating it. Using different InSAR data and techniques, it is easy to extract deformation measurements over a large area in less time.

By using appropriate knowledge of different software and techniques, deformation can be monitored accurately. DInSAR technique is suitable where fewer data are available and PSInSAR is suitable where heaps of data are available. PSInSAR technique provides higher accuracy [105] over a wide area than DInSAR. PSInSAR technique helps to predict pointwise deformation over an area, where large number of SAR data are available. Good coherence, smaller temporal baseline and shorter perpendicular baseline give good results during data processing, due to less geometric and temporal decorrelation in the constituent images.

Further research regarding advanced techniques using data from future satellite programs will undoubtedly improve the methods of deformation monitoring.

**Acknowledgements** The authors are thankful to European Space Agency for valuable information.

## References

- DiPietro, J. A. (2013). Component. *Landscape evolution in the United States* (pp. 29–40). Amsterdam: Elsevier.
- Fulton, A. (2000). *Land subsidence: What is it and important aspect of groundwater management*. Sacramento: California Department of Water Resources.
- Galloway, D. L., Jones, D. R., & Ingebritsen, S. E. (2000). *Land subsidence in the United States* (pp. 165–200). Reston: US Geological Survey Fact Sheet.
- Ishwar, S. G., & Kumar, D. (2017). Application of DInSAR in mine surface subsidence monitoring and prediction. *Current Science*, 112(1), 46–51.
- Baek, J., Kim, S.-W., Park, H.-J., Jung, H.-S., Kim, K.-D., & Kim, J. W. (2008). Analysis of ground subsidence in coal mining area using SAR interferometry. *Geosciences Journal*, 12(3), 277–284.
- Perski Z., & Jura D. (2003). Identification and measurement of mining subsidence with SAR interferometry: Potentials and limitations. In *Proceedings, 11th FIG Symposium on Deformation Measurements, Santorini, Greece* (pp. 1–7).
- What is mine subsidence?—about mine subsidence—Illinois mine subsidence insurance fund. <https://www.imsif.com/about-mine-subsidence/what-is-mine-subsidence>. Accessed 04 February 2019.
- Rajak, T. K., Yadu, L., Chouksey, S. K., & Dewangan, P. K. (2018). Stability analysis of mine overburden dump stabilized with fly ash. *International Journal of Geotechnical Engineering*, 00(00), 1–11.
- Sahu, P., & Lokhande, R. D. (2015). An investigation of sink-hole subsidence and its preventive measures in underground coal mining. *Procedia Earth and Planetary Science*, 11, 63–75.
- Jiang, L., Lin, H., Ma, J., Kong, B., & Wang, Y. (2011). Potential of small-baseline SAR interferometry for monitoring land subsidence related to underground coal fires: Wuda (Northern China) case study. *Remote Sensing of Environment*, 115(2), 257–268.
- Perski, Z. (2000). The interpretation of Ers-1 and Ers-2 insar data for the mining subsidence monitoring in upper Silesian coal basin, Poland. *International Archives of Photogrammetry and Remote Sensing*, XXXIII, 1137–1141.
- Raucoules, D., Colesanti, C., & Carnec, C. (2007). Use of SAR interferometry for detecting and assessing ground subsidence. *Comptes Rendus Geoscience*, 339(5), 289–302.
- Jian, W., Xiangguo, P., Chang Hui, X., Wang, J., Peng, X., Xu, C. H., & Chang Hui, X. (2011). Coal mining GPS subsidence monitoring technology and its application. *Mining Science and Technology (China)*, 21(4), 463–467. <https://doi.org/10.1016/j.mstc.2011.06.001>.
- Armenakis, C. (1983). Subsidence determination by aerial photogrammetry. *Geodesy and Geomatics Engineering*, 93, 1–118.
- McClusky, S., & Tregoning, P. (2013). *Background paper on subsidence monitoring and measurement with a focus on coal seam gas (CSG) activities* (pp. 1–43). Canberra: NSW Chief Scientist and Engineer.
- Thapa, S., Chatterjee, R. S., Singh, K. B., & Kumar, D. (2016). Land subsidence monitoring using Ps-InSAR technique for L-band SAR data. *ISPRS International Archives of the Photogrammetry, Remote Sensing and Spatial Information Sciences*, XLI-B7, 995–997.
- Adam, N., Kampes, B., & Eineder, M. (2005). Development of a scientific permanent scatterer system: Modifications for mixed ERS/ENVISAT time series. *European Space Agency ESA SP*, 572, 457–465. (**Special Publication**).
- Chang, H. C. C. H. C., Ge, L. G. L., & Rizos, C. (2005). DInSAR for mine subsidence monitoring using multi-source satellite SAR images. *Proceedings. 2005 IEEE International Geoscience and Remote Sensing Symposium IGARSS'05*, 3(3), 259–266.
- Moreira, A. (2013). 4th Advanced training course in Land Remote Sensing on SAR principles and applications. *German Aerospace Center (DLR)*, 4, 1–62.
- Devanathéry, N., Crosetto, M., Monserrat, O., Cuevas-González, M., & Crippa, B. (2018). Deformation monitoring using Sentinel-1 SAR data. *Multidisciplinary Digital Publishing Institute Proceedings*, 2(7), 344.
- Graham, L. C. (1974). Synthetic interferometer radar for topographic mapping. *Proceedings of the IEEE*, 62(6), 763–768.
- Stewart, R. H. (1988). Seasat: Results of the mission. *Bulletin of the American Meteorological Society*, 69(12), 1441–1447.
- Griffiths, H. (1995). Interferometric synthetic aperture radar. *Electronics and Communication Engineering Journal*, 7(6), 247.
- Yang, C., Zhang, Q., Zhao, C., Ji, L., & Zhu, W. (2010). Monitoring mine collapse by D-InSAR. *Mining Science and Technology (China)*, 20(5), 696–700.
- Qiu, Z., Ma, Y., & Guo, X. (2016). Atmospheric phase screen correction in ground-based SAR with PS technique. *Springer-plus*, 5(1), 1–15.

26. Suresh, D., & Yarrakula, K. (2018). Subsidence monitoring techniques in coal mining: Indian scenario. *Indian Journal Geomarine Science*, 47(10), 1918–1933.
27. Massonnet, D., Holzer, T., & Vadon, H. (1997). Land subsidence caused by the East Mesa geothermal field, California, observed using SAR interferometry. *Geophysical Research Letters*, 24(8), 901–904.
28. Luo, Q., Zhou, G., & Perissin, D. (2017). Monitoring of subsidence along Jingjin Inter-City railway with high-resolution terraSAR-X MT-InSAR analysis. *Remote Sensing*, 9(7), 717.
29. Ullo, S. L., Addabbo, P., Di Martire, D., Sica, S., Fiscante, N., Cicala, L., & Angelino, C. V. (2019). Application of DInSAR Technique to High Coherence Sentinel-1 Images for Dam Monitoring and Result Validation Through in Situ Measurements. *IEEE Journal of Selected Topics in Applied Earth Observations and Remote Sensing*, 12(3), 875–890. <https://doi.org/10.1109/JSTARS.2019.2896989>.
30. Kumar, S., Garg, R. D., Govil, H., & Kushwaha, S. P. S. (2019). PolSAR-decomposition-based extended water cloud modeling for forest aboveground biomass estimation. *Remote Sensing*, 11(19), 1–27.
31. Monitoring satellites. [https://www.cnpm.embrapa.br/projetos/sat/conteudo/missao\\_radarsat.html](https://www.cnpm.embrapa.br/projetos/sat/conteudo/missao_radarsat.html). Accessed 13 October 2017.
32. Kumar, S., Joshi, S. K., & Govil, H. (2017). Spaceborne PolSAR tomography for forest height retrieval. *IEEE Journal of Selected Topics in Applied Earth Observations and Remote Sensing*, 10(12), 5175–5185.
33. Samsonov, S. V., Tiampo, K. F., & Feng, W. (2016). Fast subsidence in downtown of Seattle observed with satellite radar. *Remote Sensing Applications: Society and Environment*, 4, 179–187.
34. Khan A., Govil H., Kumar G., & Dave R. (2020). Synergistic use of Sentinel-1 and Sentinel-2 for improved LULC mapping with special reference to bad land class: A case study for Yamuna river floodplain, India. *Spatial Information Research*, 1–13. <https://doi.org/10.1007/s41324-020-00325-x>.
35. Radar Image Distortions [WWW Document]. (2016). Natural Resources Canada. <https://www.asf.alaska.edu/asf-tutorials/sar-basics/>. Accessed 17 Jan 2019.
36. Way, J., Evans, D., & Elachi, C. (1994). THE SIR-C/X-SAR MISSION. In *Proceedings of IGARSS '93 - IEEE International Geoscience and Remote Sensing Symposium* (p. 593). IEEE. <https://doi.org/10.1109/igarss.1993.322262>.
37. Wolfe, W. L. (2009). *Applications overview*. Dehradun: IIRS.
38. Campbell, D. B., Jurgens, R. F., Dyce, R. B., Harris, F. S., & Pettengill, G. H. (1970). Radar interferometric observations of venus at 70-centimeter wavelength. *Science*, 170(3962), 1090–1092.
39. Shapiro I. I., Zisk S. H., Rogers A. E. E., Slade M. A., & Thompson T. W. (1972). Lunar topography: Global determination. *Science*, 178, 939–948.
40. Woodhouse, I. H. (2006). *Introduction to microwave remote sensing* (p. 126). Milton: Taylor & Francis.
41. Bamler, R., & Hartl, P. (1998). Synthetic aperture radar interferometry. *Inverse Problems*, 14(4), 55.
42. Ferretti, A., Monti-guarnieri, A., Prati, C., & Rocca, F. (2007). InSAR Principles: Guidelines for SAR Interferometry Processing and Interpretation [WWW Document]. ESA Publications. [https://www.esa.int/esapub/tm/19/TM-19\\_ptA.pdf](https://www.esa.int/esapub/tm/19/TM-19_ptA.pdf). Accessed 27 May 2017.
43. Zhou, X., Chang, N., & Li, S. (2009). Applications of SAR Interferometry in earth and environmental science research. *Sensors*, 9(3), 1876–1912.
44. Wdowski, S., Kim, S., Amelung, F., & Dixon, T. (2006). Wetland InSAR. In *AGU Fall Meeting Abstracts* (pp. H24C–07).
45. Liew S. C. (2001). Principles of remote sensin—centre for remote imaging, sensing and processing, CRISP. *Interpreting Optical Remote Sensing Images*. <https://crisp.nus.edu.sg/~research/tutorial/intro.htm>. Accessed 29 August 2017.
46. ESA. (2009). Synthetic aperture radar land applications-tutorial. *ESA Special Publication*. [https://earth.esa.int/documents/10174/2700124/sar\\_land\\_apps\\_1\\_theory.pdf](https://earth.esa.int/documents/10174/2700124/sar_land_apps_1_theory.pdf). Accessed 26 April 2018.
47. Muirhead, F., Woodhouse, I. H., & Mulgrew, B. (2016). Airborne X-band SAR tomography for forest volumes. In *SAR Image Analysis, Modeling, and Techniques XVI, SPIE* (pp. 1000308). <https://doi.org/10.1117/12.2240645>.
48. Monika, Govil, H., Chatterjee, R. S., Tripathi, M. K., Malik, K., & Diwan, P. (2018). Identification and measurement of deformation using sentinel data and PsInSAR technique in coalmines of Korba. *ISPRS - International Archives of the Photogrammetry, Remote Sensing and Spatial Information Sciences, XLII-5*(November), 427–431. <https://doi.org/10.5194/isprs-archives-xlii-5-427-2018>.
49. Hess, L. L., Melack, J. M., & Simonett, D. S. (1990). Radar detection of flooding beneath the forest canopy: A review. *International Journal of Remote Sensing*, 11(7), 1313–1325.
50. Homer, J., Longstaff, I. D., & Callaghan, G. (1996). Multi-baseline interferometry. *International Geoscience and Remote Sensing Symposium*, 1, 796–798.
51. Manunta, M. (2009). *New advances in multi-temporal differential SAR interferometry for full resolution data analysis*. Cagliari: University of Cagliari.
52. van Zyl, J. J., & Kim, Y. (2000). The relationship between radar polarimetric and interferometric phase. *IGARSS 2000. IEEE 2000. International Geoscience and Remote Sensing Symposium. Proceedings*, 3, 1301–1303.
53. Short, N., Brisco, B., & Murnaghan, K. (2011). InSAR Measurements of Terrain Stability in Canada's North [WWW Document]. Natural Resources Canada. [http://www.nrcan.gc.ca/sites/www.nrcan.gc.ca/files/earth-sciences/files/pdf/geomatics/insar\\_north-eng.pdf](http://www.nrcan.gc.ca/sites/www.nrcan.gc.ca/files/earth-sciences/files/pdf/geomatics/insar_north-eng.pdf). Accessed 14 Sept 2017.
54. Samieie-esfahany, S., Hanssen, R. F., Thienen-visser, K. Van, Muntendam-bos, A., Samiei-Esfahany, S., Hanssen, R. F., & Muntendam-bos, A. (2010). On the effect of horizontal deformation on InSAR subsidence estimates. In *Proceedings of the Fringe 2009 Workshop, 2009* (March) (pp. 1–7). Retrieved from [https://earth.esa.int/workshops/fringe09/proceedings/papers/s12\\_3esfa.pdf](https://earth.esa.int/workshops/fringe09/proceedings/papers/s12_3esfa.pdf).
55. Hanssen, R. F. (2005). Satellite radar interferometry for deformation monitoring: A priori assessment of feasibility and accuracy. *International Journal of Applied Earth Observation and Geoinformation*, 6(3–4), 253–260.
56. Campbell, D. B., Jurgens, R. F., Dyce, R. B., Harris, F. S., & Pettengill, G. H. (1970). Radar Interferometric Observation of Venus at 70-Centimeter Wavelength. *Science*, 170(3962), 1090–1092. <https://doi.org/10.1126/science.170.3962.1090>.
57. Gabriel, A. K., Goldstein, R. M., & Zebker, H. A. (1989). Mapping small elevation changes over large areas: Differential radar interferometry. *Journal of Geophysical Research: Solid Earth*, 94(B7), 9183–9191.
58. Galloway D. L., Jones D. R., & Ingebritsen S. E. (2000). Measuring land subsidence from Space. GS Fact Sheet-051-00. <https://pubs.usgs.gov/fs/fs-051-00/pdf/fs-051-00.pdf>. Accessed 04 November 2017.
59. Geudtner, D., Prats-Iraola, P., Shau, R., Bamler, R., Rodriguez Gonzalez, F., Yague-Martinez, N., & Eineder, M. (2016). Interferometric processing of Sentinel-1 TOPS data. *IEEE Transactions on Geoscience and Remote Sensing*, 54(4), 2220–2234. <https://doi.org/10.1109/tgrs.2015.2497902>.
60. Moreira, A., Prats-Iraola, P., Younis, M., Krieger, G., Hajnsek, I., & Papathanassiou, K. P. (2013). A tutorial on synthetic



- aperture radar. *IEEE Geoscience and Remote Sensing Magazine*, 1(1), 6–43.
61. Rosen, P. A., Hensley, S., Joughin, I. R., Li, F. K., Madsen, S. N., Rodriguez, E., & Goldstein, R. M. (2000). Synthetic aperture radar interferometry. *Proceedings of the IEEE*, 88(3), 333–382. <https://doi.org/10.1109/5.838084>.
  62. Keydel W. (2007). Normal and differential SAR interferometry. *Radar Polarimetry and Interferometry*, 3-1-3–36.
  63. Pinel, V., & Raucoules, D. (2016). The contribution of SAR data to volcanology and subsidence studies. *Land surface remote sensing* (pp. 221–262). Amsterdam: Elsevier.
  64. Casagli, N., Cigna, F., Bianchini, S., Hölbling, D., Füreder, P., Righini, G., & Bianchi, M. (2016). Landslide mapping and monitoring by using radar and optical remote sensing: Examples from the EC-FP7 project SAFER. *Remote Sensing Applications: Society and Environment*, 4(7), 92–108. <https://doi.org/10.1016/j.rsase.2016.07.001>.
  65. Bonì, R., Meisina, C., Perotti, C., & Fenaroli, F. (2015). PSI-based methodology to land subsidence mechanism recognition. *Proceedings of the International Association of Hydrological Sciences*, 372, 357–360.
  66. Monika, Govil, H., Chatterjee, R. S., Tripathi, M. K., Malik, K., Diwan, P., & Gill, N. (2018). Deformation monitoring in and around the national capital region of india using dinsar technique. *ISPRS - International Archives of the Photogrammetry, Remote Sensing and Spatial. Information Sciences, XLII-5*, 427–431. <https://doi.org/10.5194/isprs-archives-xxlii-5-433-2018>.
  67. Gonnuru, P., & Kumar, S. (2018). PsInSAR based land subsidence estimation of Burgan oil field using TerraSAR-X data. *Remote Sensing Applications: Society and Environment*, 9, 17–25.
  68. Paillou, P., Lopez, S., Farr, T., & Rosenqvist, A. (2010). Mapping subsurface geology in Sahara using L-band SAR: First results from the ALOS/PALSAR imaging radar. *IEEE Journal of Selected Topics in Applied Earth Observations and Remote Sensing*, 3(4), 632–636.
  69. Fletcher K., Ferretti A., Monti-guarnieri A., Prati C., Rocca F. (2007). InSAR principles: Guidelines for SAR interferometry processing and interpretation(ESA TM-19)/ESA Publications/About Us/ESA. *ESA Publications*. [https://www.esa.int/About\\_Us/ESA\\_Publications/InSAR\\_Principles\\_Guidelines\\_for\\_SAR\\_Interferometry\\_Processing\\_and\\_Interpretation\\_br\\_ESA\\_TM-19](https://www.esa.int/About_Us/ESA_Publications/InSAR_Principles_Guidelines_for_SAR_Interferometry_Processing_and_Interpretation_br_ESA_TM-19). Accessed 27 May 2017.
  70. Simons, M., & Rosen, P. A. (2007). Interferometric synthetic aperture radar geodesy. *Treatise on Geophysics*, 3, 391–446.
  71. Oliver, C. J. (1989). Synthetic-aperture radar imaging. *Journal of Applied Physics*, 22, 871–890.
  72. Feigl, K. L., Massonnet, D., & Feigl, K. L. (1998). Radar interferometry and its application to changes in the Earth's surface. *Reviews of Geophysics*, 36(4), 441–500.
  73. Devanthery, N., Crosetto, M., Cuevas-González, M., Monserrat, O., Barra, A., & Crippa, B. (2016). Deformation monitoring using persistent scatterer interferometry and Sentinel-1 SAR data. *Procedia Computer Science*, 100(100), 1121–1126.
  74. Ferretti, A., Prati, C., & Rocca, F. (2001). Permanent scatterers in SAR interferometry. *IEEE Transactions on Geoscience and Remote Sensing*, 39(1), 8–20.
  75. Ferretti, A., Prati, C., & Rocca, F. (2000). Analysis of permanent scatterers in SAR interferometry. *IGARSS 2000. IEEE 2000 International Geoscience and Remote Sensing Symposium. Taking the Pulse of the Planet: The Role of Remote Sensing in Managing the Environment*, 2, 761–763. (Cat. No. 00CH37120).
  76. Ferretti, A., Monti-guarnieri, A., Prati, C., Rocca, F., & Massonnet, D. (CNES). (2007). *InSAR processing: A mathematical approach (Part C)*. In *InSAR Principles: Guidelines for SAR Interferometry Processing and Interpretation* (pp. 120–234).
  77. Grzovic, M., & Ghulam, A. (2015). Evaluation of land subsidence from underground coal mining using TimeSAR (SBAS and PSI) in Springfield, Illinois, USA. *Natural Hazards*, 79(3), 1739–1751.
  78. Abdikan, S., Arikan, M., Sanli, F. B., & Cakir, Z. (2014). Monitoring of coal mining subsidence in peri-urban area of Zonguldak city (NW Turkey) with persistent scatterer interferometry using ALOS-PALSAR. *Environmental Earth Science*, 71(9), 4081–4089.
  79. Overview | ROI\_PAC: Open Source InSAR software | ROI\_PAC at Cornell University. [https://www.geo.cornell.edu/eas/PeoplePlaces/Faculty/matt/roi\\_pac.html/](https://www.geo.cornell.edu/eas/PeoplePlaces/Faculty/matt/roi_pac.html/). Accessed 13 October 2017.
  80. Di Martire, D., Iglesias, R., Monells, D., Centolanza, G., Sica, S., Ramondini, M., & Calcaterra, D. (2014). Comparison between Differential SAR interferometry and ground measurements data in the displacement monitoring of the earth-dam of Conza della Campania (Italy). *Remote Sensing of Environment*, 148, 58–69. <https://doi.org/10.1016/j.rse.2014.03.014>.
  81. Maheshwari, R. (2016). *Delineation and characterization of Chambal ravines using SAR interferometry and geospatial techniques*. Vanasthali: Banasthali University.
  82. Bisceglie, M., Di Santo, M., Lanari, R., & Ranaldo, N. (2010). Synthetic aperture radar processing with GPGPU. *IEEE Signal Processing Magazine*, 27, 69–78.
  83. Werner, C., & Wegmüller, U. (2006). Gamma Sar and interferometry software. *Data Processing 16.1*, 1–4.
  84. Werner, C., Wegmüller, U., Strozzi, T., & Wiesmann, A. (2000). Gamma SAR and interferometric processing software. *Proceedings of the Ers-Envisat Symposium, Gothenburg, Sweden*, 1620, 1620.
  85. Mohammad, D., Haque, E., Van Der Meijde, M., & Van Der Werff, H. (2016). *3-D surface deformation model from sub-pixel correlation of optical imagery and InSAR*. Enschede: University of Twente.
  86. Home | PolSARpro | ESA. <https://earth.esa.int/web/polsarpro>. Accessed 22 October 2017.
  87. Morishita, Y., Lazecky, M., Wright, T. J., Weiss, J. R., Elliott, J. R., & Hooper, A. (2020). LiCSBAS: An open-source insar time series analysis package integrated with the LiCSAR automated sentinel-1 InSAR processor. *Remote Sensing*, 12(3), 6–13.
  88. Qin Y., & Perissin D. (2015). Monitoring underground mining subsidence in South Indiana with C- and L-band InSAR technique. In *2015 IEEE International Geoscience and Remote Sensing Symposium (IGARSS)* (pp. 294–297).
  89. Perissin, D., Wang, Z., Prati, C., & Rocca, F. (2013). Terrain monitoring in China via ps-qps insar: Tibet and the three gorges dam. *European Space Agency (Special Publication) ESA SP*, 704, 2–6.
  90. Perissin, D. (2009). Sarproz [WWW Document]. Sarproz.Com. <https://sarproz.com/publish/SARPROZ.pdf>. Accessed 14 July 2017.
  91. Synthetic aperture RADAR (SAR) remote sensing basics and applications—Part 2 | GeoSpatial Warehouse. <https://geospatialwarehouse.com/2019/10/20/synthetic-aperture-radar-sar-remote-sensing-basics-and-applications-part-2/>. Accessed 02 November 2019.
  92. Gabriel, A. K., Goldstein, R. M., & Zebker, H. A. (1989). Mapping small elevation changes over large areas: Differential radar interferometry. *Journal of Geophysical Research*, 94(B7), 9183–9191.
  93. Mangla, R., & Kumar, S. (2014). DEM construction using DINSAR. *International Archives of the Photogrammetry*,



- Remote Sensing and Spatial Information Sciences—ISPRS Archives*, XL-8(1), 817–820.
94. Aydoner, C., Maktav, D., & Alparslan, E. (2004). Ground deformation mapping using InSAR. *ISPRS Congress Technical Commission, I*, 120–123.
  95. Guang L., Huadong G., Jinghui F., Xiaofang G., Perski Z., & Huanyin Y. (2009) Mining area subsidence monitoring using Multi-band SAR data. In *IEEE* (pp. 1–6).
  96. Raspini, F., Ciampalini, A., Del Conte, S., Lombardi, L., Nocentini, M., Gigli, G., & Casagli, N. (2015). Exploitation of amplitude and phase of satellite SAR images for landslide mapping: The case of Montescaglioso (South Italy). *Remote Sensing*, 7(11), 14576–14596. <https://doi.org/10.3390/rs71114576>.
  97. Devanthery, N., Crosetto, M., Monserrat, O., Cuevas-González, M., & Crippa, B. (2018). Deformation monitoring using Sentinel-1 SAR data. *Proceedings*, 2(7), 344.
  98. Imamoglu, M., Kahraman, F., Cakir, Z., & Sanli, F. B. (2019). Ground deformation analysis of Bolvadin (W. Turkey) by means of multi-temporal InSAR techniques and Sentinel-1 data. *Remote Sensing*, 11(9), 1–17.
  99. Azadnejad, S., Maghsoudi, Y., & Perissin, D. (2019). Evaluation of polarimetric capabilities of dual polarized Sentinel-1 and TerraSAR-X data to improve the PSInSAR algorithm using amplitude dispersion index optimization. *International Journal of Applied Earth Observation and Geoinformation*, 84, 1–11. <https://doi.org/10.1016/j.jag.2019.101950>.
  100. Govil, H., Monika, Tripathi, M. K., & Guha, S., (2019). Deformation monitoring using D-InSAR technique in coalfield of Korba Chhattisgarh, India. In *Proceedings of the 16th International Conference on Electrical Engineering/Electronics, Computer, Telecommunications and Information Technology, ECTI-CON 2019*, (January 2020) (pp. 681–684). <https://doi.org/10.1109/ECTI-CON47248.2019.8955390>.
  101. Pieraccini M., Papi F., & Rocchio S. (2015). SAR imagery by RotoSAR. In *2015 IEEE International Conference on Microwaves, Communications, Antennas and Electronic Systems, COMCAS 2015* (pp. 1–5).
  102. Kim, J. W. (2013). *Applications of Synthetic Aperture Radar (SAR)/ SAR Interferometry (InSAR) for Monitoring of Wetland Water Level and Land Subsidence* (pp. 1–111). Ohio StateUniversity. Ohio: The Ohio State University Columbus.
  103. Ishwar, S. G., & Kumar, D. (2017). Application of DInSAR in mine surface subsidence monitoring and prediction. *Current Science*, 112, 46–51. <https://doi.org/10.18520/csv112/i01/46-51>.
  104. Chatterjee, R. S., Fruneau, B., Rudant, J. P., Roy, P. S., Frison, P.-L., Lakhera, R. C., & Saha, R. (2006). Subsidence of Kolkata (Calcutta) City, India during the 1990s as observed from space by differential synthetic aperture radar interferometry (D-InSAR) technique. *Remote Sensing of Environment*, 102(1–2), 176–185. <https://doi.org/10.1016/j.rse.2006.02.006>.
  105. Vicari, A., Famiglietti, N. A., Colangelo, G., & Cecere, G. (2019). A comparison of multi temporal interferometry techniques for landslide susceptibility assessment in urban area: An example on Stigliano (MT), a town of Southern of Italy. *Geomatics, Natural Hazards Risk*, 10(1), 836–852.

**Publisher's Note** Springer Nature remains neutral with regard to jurisdictional claims in published maps and institutional affiliations.